New Lytic Peptides Based on the D,L-Amphipathic Helix Motif Preferentially Kill Tumor Cells Compared to Normal Cells†

Niv Papo and Yechiel Shai*

Department of Biological Chemistry, The Weizmann Institute of Science, Rehovot, 76100 Israel

Received November 20, 2002; Revised Manuscript Received May 12, 2003

ABSTRACT: Despite significant advances in cancer therapy, there is an urgent need for drugs with a new mode of action that will preferentially kill cancer cells. Several cationic antimicrobial peptides, which bind strongly to negatively charged membranes, were shown to kill cancer cells slightly better than normal cells. This was explained by a slight increase (3−9%) in the level of the negatively charged membrane phosphatidylserine (PS) in many cancer cells compared to their normal counterparts. Unfortunately, however, these peptides are inactivated by serum components. Here we synthesized and investigated the anticancer activity and the role of peptide charge, peptide structure, and phospholipid headgroup charge on the activity of a new group of diastereomeric lytic peptides (containing D- and L-forms of leucine and lysine; 15−17 amino acids long). The peptides are highly toxic to cancer cells, to a degree similar to or larger than that of mitomycin C. However, compared with mitomycin C and many native antimicrobial peptides, they are more selective for cancer cells. The peptides were investigated for (i) their binding to mono- and bilayer membranes by using the surface plasmon resonance (SPR) technique, (ii) their ability to permeate membranes by using fluorescence spectroscopy, (iii) their structure and their effect on the lipid order by using ATR-FTIR spectroscopy, and (iv) their ability to bind to cancer versus normal cells by using confocal microscopy. The data suggest that the peptides disintegrate the cell membrane in a detergent-like manner. However, in contrast to native antimicrobial peptides, the diastereomers bind and permeate similarly zwitterionic and PS-containing model membranes. Therefore, cell selectivity is probably determined mainly by improved electrostatic attraction of the peptides to acidic components on the surface of cancer cells (e.g., O-glycosylation of mucines). The simple composition of the diastereomeric peptides and their stability regarding enzymatic degradation by serum components make them excellent candidates for new chemotherapeutic drugs.

Anticancer drugs can be classified into a number of families on the basis of their biochemical activities or their origin. These families include alkylating agents, antimetabolites, and natural products. Antimetabolites and alkylating agents predominantly inhibit nucleic acid synthesis and tend to be active mainly against proliferating cells, and natural products are heterogeneous in their mode of action. Most chemotherapeutic agents also affect normal mammalian cells and consequently cause severe side effects (*1*). In addition, these compounds need to penetrate into the target cell to function. As a consequence, the cell can develop resistance by pumping out the drugs using multidrug resistance proteins. Because of this, there is an urgent need to develop a new class of anticancer drugs with a new mode of action that acts preferentially on cancer cells instead of normal cells. A promising group under investigation includes cationic antimicrobial peptides, known to play an important role in the innate immunity of a diverse range of organisms, including insects, amphibians, and mammals (*2*−*4*). Most cationic antimicrobial peptides are toxic to bacteria but not to normal mammalian cells, because they can bind and permeate the negatively charged outer membrane of bacteria better than the predominantly zwitterionic membrane of normal mammalian cells (*5*, *6*).

Compared to the highly negatively charged outer surface of the bacterial membrane, the outer membrane of cancer cells contains only a small amount of negatively charged phosphatidylserine (PS)[1] (3−9%), being only slightly more negative than that of normal eukaryotic cells. Despite this, some native cationic antimicrobial peptides are more toxic to cancer cells than to normal cells, which raises the question of whether the slight difference in the membrane composition of these cells can explain their ability to preferentially kill

† Supported in part by the Israel Cancer Research Fund (ICRF), the Association of the Cure of the Cancer of Prostate (Cap CURE), and the Israel Cancer Society (ICF). Y.S. is the Harold S. and Harriet B. Brady Professorial Chair in Cancer Research.

* To whom correspondence should be addressed: Department of Biological Chemistry, The Weizmann Institute of Science, Rehovot, 76100 Israel. Telephone: 972-8-9342711. Fax: 972-8-9344112. E-mail: Yechiel.Shai@ weizmann.ac.il.

[1] Abbreviations: ATR-FTIR, attenuated total reflectance Fourier transform infrared; BHA, 4-methyl benzhydrylamine resin; Boc, butyloxycarbonyl; HF, hydrogen fluoride; hRBC, human red blood cells; LC_{50}, concentration of the peptide that causes 50% of the cells to lyse; MIC, minimal inhibitory concentration; PBS, phosphate-buffered saline; PC, egg phosphatidylcholine; PE, *E. coli* phosphatidylethanolamine; PG, egg phosphatidylglycerol; PS, bovine spinal cord phosphatidylserine; SM, sphingomyelin; chol, cholesterol; RP-HPLC, reverse-phase high-performance liquid chromatography; SUV, small unilamellar vesicles; TFA, trifluoroacetic acid; RU, resonance signal; SPR, surface plasmon resonance.

10.1021/bi027212o CCC: $25.00
Published on Web 07/19/2003

cancer cells (*7*). Limited studies were conducted with native all L-amino acid antimicrobial peptides with a defined α-helical or β-sheet secondary structure. However, native antimicrobial peptides have several limitations that prevent their application in cancer therapy, such as their inactivation in serum and sensitivity to enzymatic degradation.

Recently, we reported a new group of antibacterial peptides composed of both L- and D-amino acids (diastereomers) with promising properties that allow them to be developed for systemic use (*8*). These peptides are derived from potent non-cell selective lytic peptides by replacing a few L-amino acids with their D-enantiomers. The resulting diastereomeric peptides lose their cytotoxic effect on normal mammalian cells but preserve antibacterial activity and the ability to increase the level of permeation of negatively charged phospholipid membranes which is similar to that of native antimicrobial peptides (*8*).

In this study, we synthesized a new series of diastereomeric lytic peptides (15−17 amino acids long) and investigated their anticancer activity, structure and organization in the membrane, binding to and ability to permeate zwitterionic and negatively charged model phospholipid membranes, and binding to normal and cancer cells. This was accomplished by using ATR-FTIR and fluorescence spectroscopy, surface plasmon resonance (SPR) using mono- and bilayers, and confocal microscopy. The peptides are composed of only leucine and lysine, and one-third of their sequence consists of D-amino acids. The peptide length and the positions of the D-amino acids were such that short peptides with consecutive stretches of only one to three L-amino acids would not form amphipathic α-helical oligomers in solution and a stable helical structure in membranes. The influence of the peptide's charge on anticancer activity was tested by adding lysines to the N-terminus of the peptides. In addition, the effect of structure stability was tested by reverting to the sequence of the parental peptide. The results are discussed with respect to the parameters involved in the high toxicity and selectivity of the diastereomers toward cancer cells and their advantages over all L-amino acid peptides as potential candidates for chemotherapeutic agents with a new mode of action.

EXPERIMENTAL PROCEDURES

Materials. 4-Methyl benzhydrylamine resin (BHA) and butyloxycarbonyl (Boc) amino acids were purchased from Calibochem-Novabiochem (La Jolla, CA). Other reagents used for peptide synthesis included trifluoroacetic acid (TFA, Sigma), *N*,*N*-diisopropylethylamine (DIEA, Aldrich), methylene chloride (peptide synthesis grade, Biolab), dimethylformamide (peptide synthesis grade, Biolab), and benzotriazolyl *n*-oxy-tris(dimethylamino)phosphonium hexafluorophosphate (BOP, Sigma). Egg phosphatidylcholine (PC) was purchased from Lipid Products (South Nutfield, U.K.). Egg phosphatidylglycerol (PG), egg sphingomyelin (SM), bovine brain phosphatidylserine (PS), phosphatidylethanolamine (PE) (type V, from *Escherichia coli*), *N*-octyl β-D-glucopyranoside (OG), bovine serum albumin (BSA), insulin, testosterone, and Triton X-100 were purchased from Sigma. Cholesterol (extra pure) was supplied by Merck (Darmstadt, Germany). Calcein was purchased from Hach Chemical Co. (Loveland, CO). Dulbecco's modified Eagle's medium (DMEM), RPMI-1640 medium, heat-inactivated fetal calf serum (FCS), L-glutamine, penicillin−streptomycin nystatin antibiotics, penicillin−streptomycin antibiotics, and trypsin EDTA solution B were supplied by Biological Industries (Beit Haemek, Israel). Bovine serum was purchased from Hyclone. Anti PPLO agent was purchased from Gibco BRL. NIH-3T3 mouse and OL human foreskin fibroblasts, B16 F10 mouse melanoma, murine Lewis lung carcinoma (LLC), and human prostate carcinoma (CL1, 22RV1, and LNCaP strains) cell lines were purchased from the American Type Culture Collection (ATCC). All other reagents were analytical grade.

Cell Cultures. B16 F10 mouse melanoma, CL1, and 22RV1 human prostate carcinoma cell lines were grown in RPMI-1640 medium supplemented with 10% fetal calf serum and antibiotics, at 37 °C in a humidified atmosphere at 5% CO_2 and 95% air. Cells were treated three times per week. NIH-3T3 mouse fibroblast cell lines were grown in DMEM supplemented with 10% bovine calf serum and antibiotics under the same conditions described above. Similarly, OL human foreskin fibroblasts and murine Lewis lung carcinoma (LLC) cell lines were grown in DMEM supplemented with 10% fetal calf serum and antibiotics. LNCaP human prostate carcinoma cells were grown in a manner similar to that of CL1 but with the addition of insulin (5×10^{-3} mg/mL) and testosterone (10^{-9} M).

Peptide Synthesis and Purification. Peptides were synthesized by a solid-phase method on 4-methyl benzhydrylamine resin (0.05 mequiv) (*9*). Labeling of the N-terminus of the peptides with rhodamine was done on the resin-bound peptide as previously described (*10*). The resin-bound peptides were cleaved by hydrogen fluoride (HF) and, after HF evaporation and being washed with dry ether, extracted with a 50% acetonitrile/water mixture. The peptides were purified by RP-HPLC on a C_{18} reverse-phase Bio-Rad semipreperative column (250 mm × 10 mm, 300 Å pore size, 5 μm particle size), eluted in 50 min, using a linear gradient from 25 to 48% acetonitrile in water, both containing 0.05% TFA (v/v), at a flow rate of 1.8 mL/min. The purified peptides were shown to be homogeneous (∼98%) by analytical HPLC. The peptides were subjected to electrospray mass spectroscopy to confirm their molecular weight.

Preparation of SUV Vesicles. Small unilamellar vesicles (SUV) were prepared by sonication of PC/SM/PE/cholesterol (4.5/4.5/1/1, w/w), PC/SM/PE/PS/cholesterol (4.35/4.35/1/0.3/1, w/w) (3% PS), PC/SM/PE/PS/cholesterol (4.05/4.05/1/0.9/1, w/w) (9% PS) and PC/SM/PE/PS/cholesterol (3.5/3.5/1/2/1, w/w) (20% PS) mixtures. Briefly, dry lipid mixtures were dissolved in a $CHCl_3$/MeOH mixture (2/1, v/v). The solvents were evaporated under a nitrogen stream, and the lipids (at a concentration of 7.2 mg/mL) were resuspended in buffer by vortexing. The resulting lipid dispersion was sonicated in a bath-type sonicator (G1125SP1 sonicator, Laboratory Supplies Co., Hicksville, NY) until the turbidity had cleared. Vesicles were visualized by electron microscopy (JEOL, Tokyo, Japan) and were shown to be unilamellar with an average diameter of 20−40 nm.

Cytotoxicity Assays (XTT Proliferation Assay). A 96-well plate (Falcon) was used for this assay. Each well in the plate contained the cell suspension (90 μL) in medium without serum (1×10^4, 1×10^4, 7×10^3, 7×10^3, and 5×10^3 cells for 3T3, OL, B16, prostate carcinoma strains, and LLC,

respectively). Wells in the first and second columns served as blanks (medium only) and 100% survival controls (cells and medium only), respectively. Dulbecco's phosphate-buffered saline (10 μL) was added to the first and second columns, and the various concentrations of peptides (10 μL each), freshly prepared from the stock solution (1 mg/mL in water), were added to the remaining columns (two wells for each concentration of peptide solution). The plate was then incubated for 24 h before 50 μL of the XTT reaction solution {sodium 3′-[1-(phenylaminocarbonyl)-3,4-tetrazolium]bis(4-methoxy-6-nitro)benzenesulfonic acid hydrate and *N*-methyl dibenzopyrazine methyl sulfate, mixed in a 50/1 proportion} was added to each well. The optical density was read at a wavelength of 450 nm in an ELISA plate reader after incubation of the plates for 2 h with XTT (37 °C and 5% CO_2 and 95% air). Cell viability was determined relative to the control, and final results were recorded. The results were confirmed using replications in at least three independent experiments. The LC_{50} for each peptide was obtained from the curve of cell viability versus peptide concentration and taken from the concentration at which cell viability was 50%.

Hemolysis of Human Red Blood Cells (hRBC). Fresh hRBC were rinsed three times with PBS [35 mM phosphate buffer and 0.15 M NaCl (pH 7.3)] by centrifugation for 10 min at 800*g* and resuspended in PBS. Peptides dissolved in PBS were then added to 50 μL of a solution of the stock hRBC in PBS to reach a final volume of 100 μL [final erythrocyte concentration of 4% (v/v)]. The resulting suspension was incubated under agitation for 60 min at 37 °C. The samples were then centrifuged at 800*g* for 10 min. Measuring the absorbance of the supernatant at 540 nm monitored release of hemoglobin. Controls for zero hemolysis (blank) and 100% hemolysis consisted of hRBC suspended in PBS and Triton 1%, respectively.

Membrane Permeability Studies. Calcein (60 mM, self-quenching concentration) was entrapped in vesicles composed of PC, SM, PE, and cholesterol (4.5/4.5/1/1, w/w) or PC, SM, PE, PS, and cholesterol with the following ratios: 4.35/4.35/1/0.3/1 (w/w) (3% PS), 4.05/4.05/1/0.9/1 (w/w) (9% PS), and 3.5/3.5/1/2/1 (w/w) (20% PS). The buffer was 10 mM Hepes and 150 mM NaCl (pH 7.4). The nonencapsulated calcein was removed from the liposome suspension by gel filtration, using a Sephadex G-50 (Pharmacia) column connected to a low-pressure LC system (Pharmacia). Peptides were added to vesicle suspensions (2 mL, 2.4 μM liposomes), and peptide-induced calcein leakage resulted in an increase in fluorescence (*11*), and was monitored at room temperature ($\lambda_{ex} = 485$ nm, $\lambda_{em} = 515$ nm). Complete dye release (used as 100% activity) was obtained after the vesicles were disrupted with Triton X-100 (final concentration of 0.1%). Under the experimental conditions, in the absence of peptide, the leakage rate was less than 1% in 5 h.

ATR-FTIR Measurements. Spectra were obtained with a Bruker equinox 55 FTIR spectrometer equipped with a deuterated triglyceride sulfate (DTGS) detector and coupled with an ATR device as previously described (*12*). Prior to sample preparations, the trifluoroacetate (CF_3COO^-) counterions which strongly associate with the peptide were replaced with chloride ions through several lyophilizations of the peptides in 0.1 M HCl to eliminate the absorption band near 1673 cm^{-1} (*13*). Peptide incorporation into lipids and deuterium exchange were carried out as previously described in detail (*12*). Spectra were recorded by using a ZnSe prism.

ATR-FTIR Data Analysis. Spectra were processed using PEAKFIT (Jandel Scientific, San Rafael, CA) software as previously described. Second-derivative spectra accompanied by 13-data point Savitsky−Golay smoothing were calculated to identify the positions of the component bands in the spectra. These wavenumbers were used as initial parameters for curve fitting with Gaussian component peaks, and the relative areas of individual peaks, assigned to particular secondary structure. The results of four independent experiments were averaged. The analysis of the polarized ATR-FTIR spectra was carried out as described previously (*14*, *15*).

Binding Analysis by Surface Plasmon Resonance. Biosensor experiments were carried out with a BIAcore X analytical system (BIAcore, Uppsala, Sweden) using HPA and L1 sensor chips (BIAcore). The HPA sensor chip is composed of aliphatic chains covalently bound to a gold surface. A hybrid lipid monolayer is formed when the chip is in contact with vesicles. The L1 sensor chip contains hydrophobic aliphatic chains that contain exposed polar headgroups. Thus, when the chip is in contact with vesicles, a lipid bilayer is formed. We performed the protocol described previously (*16*). The running buffer used for all experiments was PBS (pH 6.8). The washing solution was the nonionic detergent *N*-octyl β-D-glucopyranoside at 40 mM. All solutions were freshly prepared, degassed, and filtered through 0.22 μm pores. The operating temperature was 25 °C. After cleaning as indicated by the manufacturers had been carried out, the BIAcore X instrument was left running overnight using Milli-Q water as an eluent to thoroughly wash all liquid handling parts of the instrument. The HPA (or L1) chip was then installed, and the alkanethiol surface was cleaned with an injection of 40 mM *N*-octyl β-D-glucopyranoside (25 μL), at a flow rate of 5 μL/min. PC/SM/PE/cholesterol (4.5/4.5/1/1, w/w) or PC/SM/PE/PS/cholesterol with PS fixed at 3, 9, and 20% (80 μL, 0.5 mM) were then applied to the chip surface at a low flow rate (2 μL/min). To remove any multilamellar structures from the lipid surface, NaOH (50 μL, 10 mM) was injected at a flow rate of 50 μL/min, or alternatively, the flow rate of the buffer alone was increased to 100 μL/min, which resulted in a stable baseline corresponding to the lipid monolayer (or bilayer) linked to the chip surface. The negative control BSA was injected (25 μL, 0.1 mg/μL in PBS) to confirm complete coverage of the nonspecific binding sites. The monolayer (or bilayer) linked to the chip surface was then used as a model cell membrane surface to study peptide−membrane binding.

Peptide solutions (15 μL of PBS solution containing 7.5−100 μM peptide) were injected onto the lipid surface at a flow rate of 5 μL/min. PBS alone then replaced the peptide solution for 25 min to allow peptide dissociation. Analysis of the peptide−lipid binding event was performed from a series of sensorgrams collected at seven different peptide concentrations. Surface plasmon resonance (SPR) detects changes in the optical properties of the sensor surface caused by the association and dissociation of the analyte from the ligand immobilized onto the sensor surface. More explicitly, the SPR phenomenon can be visualized at a particular angle of incident light. The incident angle depends on the adsorbed

Table 1: Sequences, Designations, and Net Charges of the Peptides

Peptide Designation	Sequence[a]	Net charge
$l^{3,10,13}k^{7,8}K_6L_9$	K L **L** K L L **K** **K** L **L** K L **L** L K – NH_2	+7
K-$l^{3,10,13}k^{7,8}K_6L_9$	K K L **L** K L L **K** **K** L **L** K L **L** L K – NH_2	+8
KK-$l^{3,10,13}k^{7,8}K_6L_9$	K K K L **L** K L L **K** **K** L **L** K L **L** L K – NH_2	+9
$l^{3,6,13}k^{8,9}K_6L_9$	K L **L** L K **L** L **K** **K** L L K **L** L K – NH_2	+7
LL37	LLGDFFRKSKEKIGKEFKRIVQRIKDFLRNLVPRTES–NH_2	+5
Melittin Diastereomer	G I G A **V** L K **V** L T T G L P A L **I** S W I **K** R K R Q Q-NH_2	

[a] Bold and underlined letters are D-amino acids.

mass on the sensor surface. Therefore, when the analyte is injected over the surface in a continuous flow, it adsorbs onto the immobilized ligand, thus changing the incident angle by modifying the refractive index at the surface of the sensor chip. The resulting sensorgram is a plot of the SPR signal (RU, reflected by light intensity and measured slightly below the resonance angle) against time, which allows the binding event between the analyte and the ligand to be followed, and can be used to gain information about the binding kinetics of the interaction as well as RU_{max}, the maximal response unit (or equilibrium binding response) under a steady-state condition (*17*).

Our system reached binding equilibrium during injection of the sample, and therefore, the affinity constant could be calculated from the relationship between the equilibrium binding response (R_{eq} or RU_{max}) and the peptide concentration (X), using a steady-state affinity model. The affinity constants were thus determined by nonlinear least-squares (NLLSQ) fitting using the following equation:

$$RU(X) = (K_A \times X \times RU_{max})/(1 + K_A \times X)$$

where X is the peptide concentration, RU_{max} is the maximal response unit (or equilibrium binding response), and K_A is the steady-state affinity constant.

Confocal Fluorescence Microscopy. Confocal images were obtained using an Olympus IX70 FV500 confocal laser scanning microscope. The $DiOC_6(3)$ and rhodamine system of filters was utilized. OL foreskin or CL1 prostate cancer cells were placed on a cover slip, and a series of images were taken before and after the addition of rhodamine-labeled peptides, using oil immersion. The setting of the photomultipliers (gain and black level) was constant for the series of images. Care was taken so that any existing photobleaching did not compromise the interpretation, and laser irradiation and other means of illumination were prevented between images. The confocal images were obtained at a resolution of 12 bits.

RESULTS

Peptide Design. Four diastereomers of linear short (15−17 amino acids long) lytic peptides composed of lysine and leucine were synthesized and investigated for their anticancer activity and a plausible mode of action. The diastereomers were designed to create a perfect amphipathic structure in their L-form based on Schiffer and Edmondson's wheel projection (*18*) (Figure 1). The sequences of the peptides, their designations, and net charges are given in Table 1. The

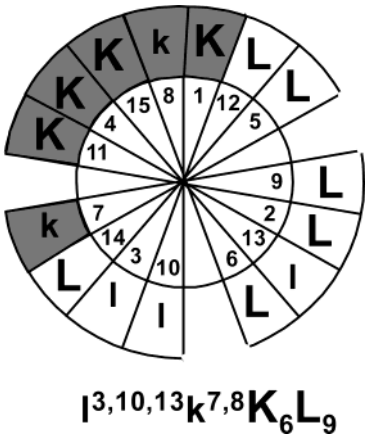

FIGURE 1: Schiffer Edmundson wheel projection (*18*) of the $l^{3,10,13}k^{7,8}K_6L_9$ diastereomer. A gray background indicates hydrophilic amino acids (Lys). A white background indicates hydrophobic amino acids (Leu), and lowercase letters indicate hydrophobic and hydrophilic D-amino acids.

peptide's length and the position of D-amino acids were such that short peptides with stretches of only one to three consecutive L-amino acids, which cannot adopt α-helical structures, were constructed. The first three peptides were designed to increase the net positive charge without altering the peptide chain, and the fourth peptide, which has the inverted sequence of the first peptide, was designed to test the effect of the peptide's dipole moment on the structure and function. The human cecropin-like antimicrobial peptide LL-37 (*19*, *20*) and a diastereomer of melittin (*21*) served as controls.

Anticancer and Hemolytic Activity of the Peptides. We tested the potential of the peptides to inhibit the growth of different cells and the extent of their hemolytic activity against the highly susceptible human erythrocytes (4% erythrocyte solution). The chemotherapeutic agent mitomycin C served as a nonpeptidic control. All the diastereomeric peptides exhibited no significant hemolytic activity toward human erythrocytes up to the maximum concentration that was tested (50 μM) (data not shown). The set of test cells included NIH-3T3 mouse fibroblasts and OL foreskin fibroblasts (both of which served to mimic noncancer cells) and five cancer cell lines (Table 2). The LC_{50} values of the peptides are also shown in Table 2. The results reveal that some of the peptides had remarkable activities and selectivity. Furthermore, compared to the diastereomers, mytomycin C cannot discriminate between cancer and NIH-3T3 cells. The most pronounced selectivity is seen with the inverted peptide, $l^{3,6,13}k^{8,9}K_6L_9$. Inversion of the sequence has an effect on the

Table 2: Lethal Concentrations (LC_{50}) of the Peptides[a]

peptide designation	NIH-3T3 mouse fibroblasts	OL foreskin fibroblasts	B16 F10 mouse melanoma	Lewis lung carcinoma (LLC)	CL1 human prostate carcinoma	22RV1 human prostate carcinoma	LNCaP human prostate carcinoma
$l^{3,10,13}k^{7,8}K_6L_9$	14	12	2.5	4.5	2.5	10	4
K-$l^{3,10,13}k^{7,8}K_6L_9$	18	16	1.5	6	1.5	2	3
KK-$l^{3,10,13}k^{7,8}K_6L_9$	16	12	1	5	1	1	1.5
$l^{3,6,13}k^{8,9}K_6L_9$	116	40	6	7.5	4	12	7.5
LL-37	28	14	12	15	6	12	ND
melittin diastereomer	>100	>50	ND	>50	>50	>50	ND
mitomycin C	3	2	3	4	5	6	8

[a] Results are the mean of three independent experiments each performed in duplicate, with the standard deviation not exceeding 20%. ND means not determined.

dipole moment of the peptide, which in turn affects the peptide structure. On the basis of the FTIR data, the inverted peptide has less α-helical structure than the wild-type peptide (discussed in the FTIR experiments). Compared to the new diastereomers, the diastereomer of melittin has no detectable activity up to 50 μM, and LL-37 is less active and less selective for cancer cells, although both are highly active toward bacteria (*21*, *22*). The data also reveal that the addition of positive charges at the N-termini of the peptide does not significantly affect their activity toward cancer cells in most cases. This is in contrast to antimicrobial activity, which usually increases upon the addition of positive charges to the N-termini of antimicrobial peptides (*5*, *23*).

Peptides Induced Calcein Leakage from Vesicles. All the peptides were tested for their potency to evoke calcein release from SUVs composed of PC/SM/PE/cholesterol (4.5/4.5/1/1, w/w) [which mimics the composition of the outer leaflet of erythrocytes (*24*)] or PC/SM/PE/PS/cholesterol in which the PS content was 3, 9, and 20% [3% PS mimics the phospholipid composition of cancer cells (*7*)]. Increasing amounts of peptides were added to a suspension of vesicles at a fixed concentration (2.4 μM). Membrane permeability was monitored by the fluorescence recovery for 45 min, and the level of maximum leakage reached as a function of the peptide-to-lipid molar ratio was determined and is shown in Figure 2. The data reveal that the peptides can only slightly discriminate between the different compositions of the vesicles. The diastereomer of melittin has been shown to be highly active only on negatively charged membranes (*21*). Interestingly, the activity of the peptides was similar whether the vesicles contained 3 or 9% PS, but lower with vesicles containing 20% PS. In addition, no significant difference in activity was observed among all of the diastereomers despite a difference in their net positive charge.

Secondary Structure of the Peptides in Zwitterionic and Negatively Charged Phospholipid Membranes, As Determined by FTIR Spectroscopy. FTIR spectroscopy was used to determine the secondary structure of the peptides bound to phospholipid membranes. Figure 3 shows, for example, the spectra of the amide I region of $l^{3,10,13}k^{7,8}K_6L_9$ bound to PC/PE/cholesterol vesicles (9/1/1, w/w) after deuteration, which is required for a better isolation of the signals as has been described previously (*25*). PG was used instead of PS, because it has a better signal at the amide I region and gives similar results in the functional assays when it replaces PS (data not shown). The assignments of the different secondary structures to the various amide I regions were calculated according to the values taken from Jackson and Mantsch (*26*). The data reveal that all the peptides besides the inverted one adopt a predominantly distorted/dynamic helix in the zwitterionic lipids (~80%), and the rest was made up of β-sheets and aggregated strands. Reverting to the sequence of $l^{3,10,13}k^{7,8}K_6L_9$ reduced its helical content by ~20% in both types of lipids, a reduction concomitant with a shift in the band from 1656 to 1658 cm^{-1}, indicating a more defined structure for the wild-type peptide. A similar reduction in the helical content was obtained in negatively charged lipids after addition of positive charges at the N-terminus of the wild-type peptide.

Orientation of the Phospholipid Membrane and Effect of Peptide Binding on the Acyl Chain Order. Polarized ATR-FTIR was used to determine the orientation of the lipid membranes and the effect of the diastereomeric peptides on the acyl chain order. The symmetric [$\nu_{sym}(CH_2) \sim 2850$ cm^{-1}] and the antisymmetric [$\nu_{antisym}(CH_2) \sim 2920$ cm^{-1}] vibrations of lipid methylene C−H bonds are perpendicular to the molecular axis of a fully extended hydrocarbon chain. Thus, measurements of the dichroism (*R*) of infrared light absorbance can reveal the order and orientation of the membrane sample relative to the prism surface. The *R* values obtained in PC/PE/cholesterol (1.15 ± 0.01) or PC/PG/PE/cholesterol (1.17 ± 0.02), at peptide-to-lipid molar ratios of both 1/120 and 1/30, indicate that the phospholipid membrane is well-ordered and predominantly in a liquid-crystalline phase, like biological cell membranes (*15*, *27*, *28*). The effect of the diastereomers on the multibilayer acyl chain order was estimated by comparing the CH_2 stretching dichroic ratio (*R*) of the pure phospholipid multibilayers with that obtained with membrane-bound diastereomers. The values obtained for all the peptides in PC/PE/cholesterol were ~1.20 and in PC/PG/PE/cholesterol ~1.23. These values indicate that the incorporation of the diastereomers into the membrane did not significantly change the order of the membrane. These data suggest that the diastereomers are localized on the surface.

Affinity of the Peptides for Lipid Monolayers and Bilayers Measured by Surface Plasmon Resonance (SPR). PC/SM/PE/cholesterol (4.5/4.5/1/1, w/w) and PC/SM/PE/PS/cholesterol (in which the PS content was 3, 9, and 20%) monolayers and bilayers were absorbed onto the HPA and L1 sensor chips, respectively. Typical sensorgrams of the binding between the peptide $l^{3,6,13}k^{8,9}K_6L_9$ and PC/SM/PE/PS/cholesterol and PC/SM/PE/cholesterol bilayers are shown in panels A and B of Figure 4, respectively. The peptide concentrations that were used were 7.5, 15, 25, 30, 50, and

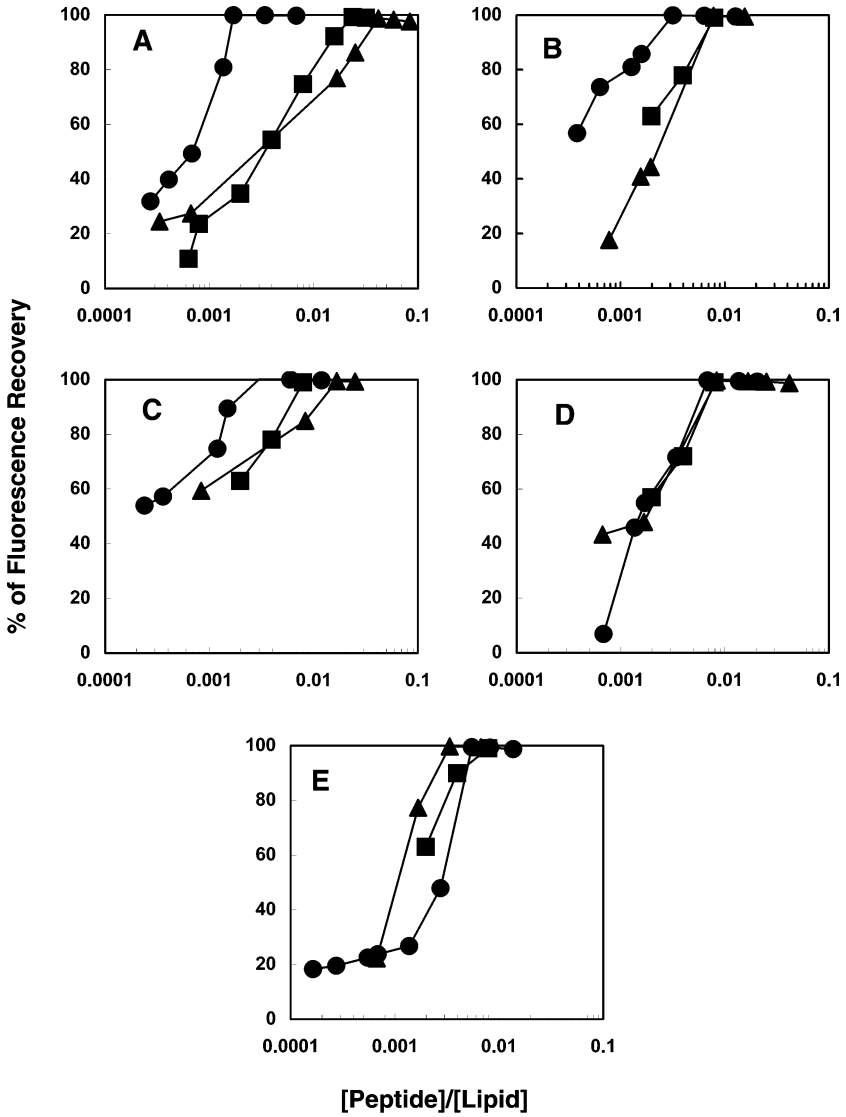

FIGURE 2: Calcein release induced by the different peptides: $l^{3,10,13}k^{7,8}K_6L_9$ (A), K-$l^{3,10,13}k^{7,8}K_6L_9$ (B), KK-$l^{3,10,13}k^{7,8}K_6L_9$ (C), $l^{3,6,13}k^{8,9}K_6L_9$ (D), and LL-37 (E). The peptides at different concentrations were added to 2.4 μM PC/SM/PE/cholesterol (4.5/4.5/1/1, w/w) (▲), PC/SM/PE/PS/cholesterol (4.05/4.05/1/0.9/1, w/w) (●), and PC/SM/PE/PS/cholesterol (3.5/3.5/1/2/1, w/w) (■) SUV containing entrapped calcein at a self-quenching concentration in 2 mL of buffer [10 mM Hepes and 150 mM NaCl (pH 7.4)]. The maximal fluorescence recovery measured after 45 min was plotted as a function of the peptide to lipid molar ratio (log scale). The results are averages of three independent repetitions with a standard deviation of 5%.

100 μM. The RU signal intensity increased as a function of the peptide's concentration, indicating that the amount of peptide bound to the lipids is proportional to the increase in peptide concentration. Figure 4 shows only a slight increase in the extent of binding when the peptide interacted with PS-containing bilayers, as compared to bilayers without PS. Similar results were obtained for all the other peptides.

Our system reached binding equilibrium during injection of the sample, and therefore, the affinity constant could be calculated from the relationship between the equilibrium binding response (R_{eq}) and the peptide concentration (C) (Figure 5), using a steady-state affinity model. The data reveal similar binding constants for binding to mono- and bilayers of zwitterionic PC/SM/PE/cholesterol membranes (Table 3). In the case of negatively charged membranes, there is a slight increase in the level of binding of the peptides to bilayers compared to that with monolayers.

It has been shown previously that partition coefficients measured by SPR are similar to those obtained by other methods (*17*, *29*). Here we verified further the validity of the SPR-derived partition coefficients by performing titration experiments with NBD-labeled $l^{3,10,13}k^{7,8}K_6L_9$. The data revealed a partition coefficient in PC/SM/PE/PS/cholesterol bilayers (4.35/4.35/1/0.3/1, w/w) of $\sim 1.65 \times 10^5$ M^{-1} (data not shown), similar to the value obtained in the BIAcore studies (Table 3).

Note that when we fitted the peptide's sensorgrams globally (using different concentrations of the peptides) with the simple 1/1 Langmuir binding model, a poor fit was obtained (data not shown). Experiments were repeated three times with a standard deviation of 5%.

Binding of a Rhodamine-Labeled Peptide to Normal and Cancer Cells As Observed by Using Confocal Fluorescence Microscopy. The wild-type peptide $l^{3,10,13}k^{7,8}K_6L_9$ was labeled with rhodamine at its N-terminus without any effect on its anticancer activity. When rhodamine-labeled peptide (2.5 μM) was added separately to OL foreskin fibroblasts (Figure 6B) or CL1 prostate cancer (Figure 6D) cells, followed by

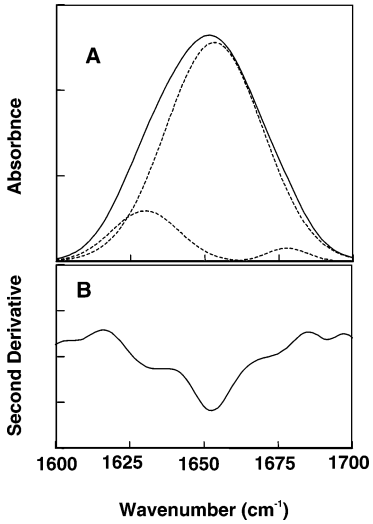

FIGURE 3: FTIR spectra deconvolution of the fully deuterated amide I band (1600−1700 cm^{-1}) of $l^{3,10,13}k^{7,8}K_6L_9$ (A) in PC/PE/Cho (9/1/1, w/w) multibilayers. Second derivatives (B) were calculated to identify the positions of the component bands in the spectra. The component peaks are the result of curve fitting using a Gaussian line shape. The sums of the fitted components can be superimposed on the experimental amide I region spectra. Continuous lines represent the experimental FTIR spectra after Savitzky−Golay smoothing; the dashed lines represent the fitted components. A 120/1 lipid/peptide molar ratio was used.

washing of the cells, we observed that the peptide binds strongly and preferentially to the CL1 cancer cells.

DISCUSSION

The interesting observation in this study is that diastereomers of cationic amphipatic α-helical peptides have potent lytic activity toward cancer cells compared to noncancer cells. In fact, their activity is similar to and even better than that of conventional chemotherapeutic agents that cannot discriminate between normal and cancer cells. Furthermore, compared to most conventional chemotherapeutic agents that act on components inside the cell, thus leaving the cell membrane intact, the diastereomers act and disintegrate the cell membrane, as revealed by their ability to bind strongly and permeate phospholipid membranes (Table 3 and Figures 2, 4, and 5) as well as their ability to lyse cells with fast kinetics (data not shown). Their drastic effect should make it more difficult for the cell to develop resistance to them.

Nonhemolytic cationic diastereomeric peptides were shown to have potent antimicrobial activity, which could be explained by their preferential binding to the highly negatively charged surface of bacteria. In agreement with this assumption, they bind and increase the permeability of negatively charged membranes that mimic bacterial membranes, significantly more than zwitterionic membranes (∼100-fold) (*5*, *30*). However, the situation is different with these diastereomers acting against cancer cells. First, the diastereomers bind only slightly better (∼2-fold) to phospholipids that mimic cancer cells than to those that mimic normal cells. Second, the wild-type peptide $l^{3,10,13}k^{7,8}K_6L_9$, is the best peptide for discriminating between negatively charged membranes and zwitterionic membranes in the calcein release assay (Figure 2A), yet it has the lowest selectivity for the cells that have been tested (Table 2). In

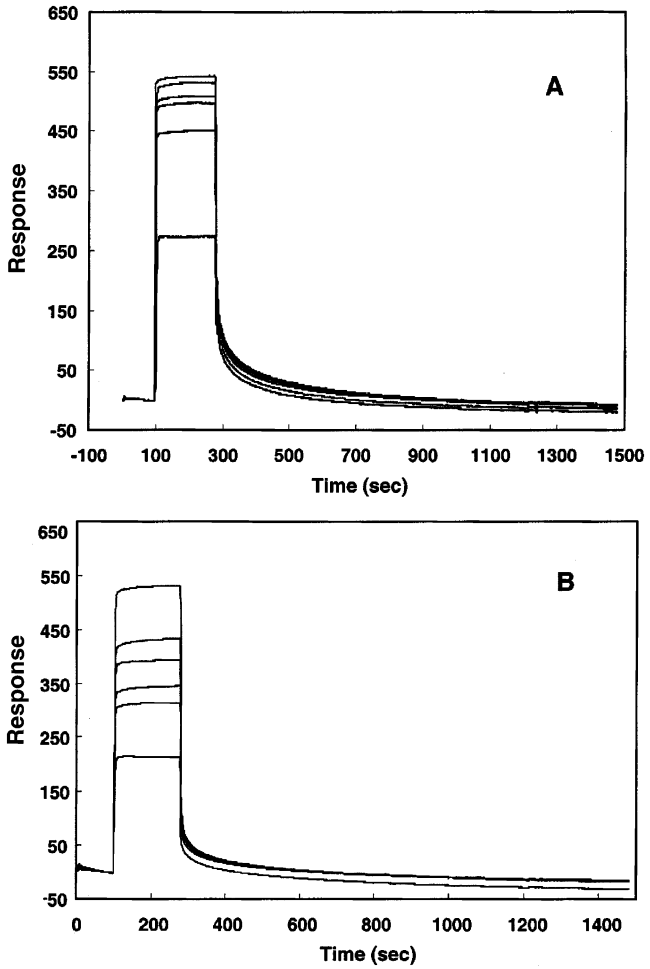

FIGURE 4: Sensorgrams of the binding between various concentrations of the peptide $l^{3,6,13}k^{8,9}K_6L_9$ and the PC/SM/PE/PS/cholesterol (4.35/4.35/1/0.3/1, w/w) (A) and PC/SM/PE/cholesterol (4.5/4.5/1/1, w/w) (B) bilayers. Peptide concentrations were 7.5, 15, 25, 30, 50, and 100 μM.

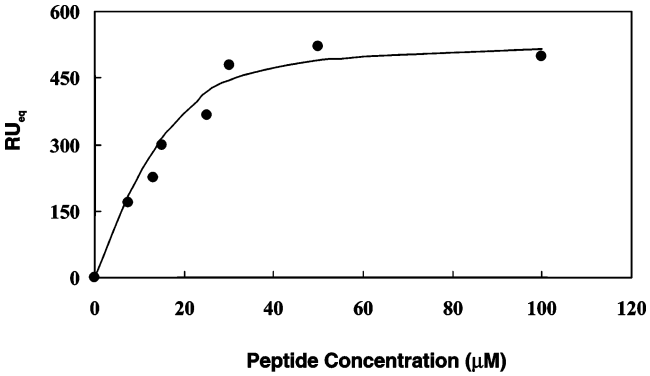

FIGURE 5: Relationship between the equilibrium binding response (RU_{eq}) and the peptide ($l^{3,6,13}k^{8,9}K_6L_9$) concentration in PC/SM/PE/cholesterol (4.5/4.5/1/1, w/w) bilayers (Figure 4B), using the BIAcore steady-state affinity model. Note that not all the points indicated are also shown in Figure 4B. Furthermore, the points that are shown are averages of at least three independent experiments.

contrast, the inverted peptide, $l^{3,6,13}k^{8,9}K_6L_9$, which cannot discriminate between the different types of phospholipids (Figure 2D), is the best one in selective activity. Confocal microscopy clearly demonstrates that the diastereomers are more active toward cancer cells because they bind them better than normal cells (Figure 6). The larger amount of the negatively charged phospholipids in the outer leaflet of

Table 3: Equilibrium Affinity Constants of the Peptides in the Presence of PC/SM/PE/Cholesterol and PC/SM/PE/PS/Cholesterol Monolayers and Bilayers According to a Steady-State Affinity Model[a]

peptide designation	K_A in PC/SM/PE/chol (4.5/4.5/1/1, w/w) (M^{-1})		K_A in PC/SM/PE/PS/chol (4.35/4.35/1/0.3/1, w/w) (M^{-1})		K_A in PC/SM/PE/PS/chol (3.5/3.5/1/2/1, w/w) (M^{-1})	
	monolayer	bilayer	monolayer	bilayer	monolayer	bilayer
$l^{3,10,13}k^{7,8}K_6L_9$	0.39×10^5	0.42×10^5	0.84×10^5	1.65×10^5	1.3×10^5	2.1×10^5
K-$l^{3,10,13}k^{7,8}K_6L_9$	0.54×10^5	0.69×10^5	1.1×10^5	2.0×10^5	2.0×10^5	3.8×10^5
KK-$l^{3,10,13}k^{7,8}K_6L_9$	0.57×10^5	0.71×10^5	1.2×10^5	2.1×10^5	2.2×10^5	3.9×10^5
$l^{3,6,13}k^{8,9}K_6L_9$	0.46×10^5	0.44×10^5	0.86×10^5	1.7×10^5	1.3×10^5	2.2×10^5

[a] The results are the average of three independent experiments with a standard deviation of 5%.

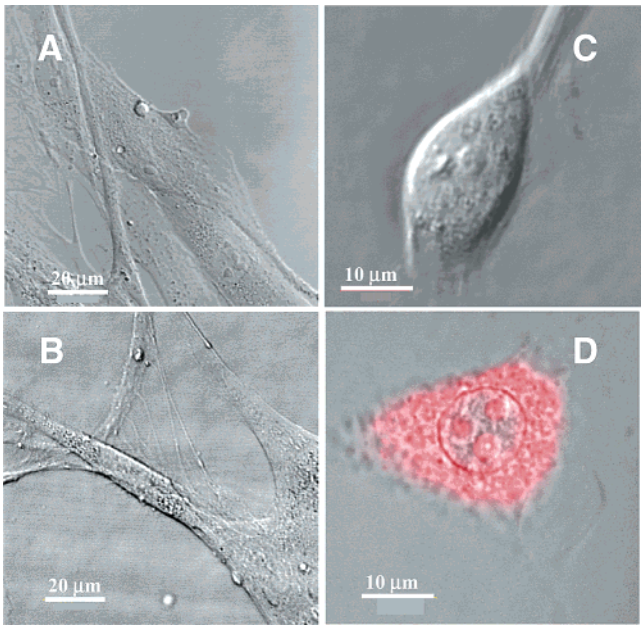

FIGURE 6: Confocal laser scanning microscopy images of normal OL foreskin and CL1 prostate cancer cells untreated (A and C, respectively) and treated (B and D, respectively) with 2.5 μM rhodamine-labeled $l^{3,10,13}k^{7,8}K_6L_9$.

cancer cells compared to that in normal cells cannot explain this selective binding and activity of the peptides toward cancer cells. This suggests that other components on the cancer cells increase the level of binding of the peptides to these cells and bring them close to the cell membrane. Indeed, many cancer cells are enriched with O-glycosylated mucines, which are high-molecular weight glycoproteins comprised of a backbone protein to which oligosaccharides are attached via the hydroxylic groups of serine or threonine (*31*). After accumulation on the cell surface, the peptides can traverse the cell membrane and permeate it, because they bind and permeate strongly zwitterionic membranes. The fact that a high affinity for both negatively charged and zwitterionic membranes is probably essential for anticancer activity is further demonstrated in the following three examples. (i) LL-37 has high affinity for both types of lipids and as a result is active on cancer cells, albeit with low selectivity. (ii) A diastereomer of melittin which binds very weakly to zwitterionic phospholipids (~1000-fold weaker than to negatively charged phospholipids) (*21*, *32*) is not active on the cancer cells that were tested, at concentrations of up to 50 μM (Table 2). (iii) Magainin, which binds ~100-fold weaker to zwitterionic than to negatively charged membranes, is active on cancer cells at only a concentration of ~25 μM (*33*). However, we cannot rule out the possibility that the higher negative potential inside cancer cells, compared to that in noncancer cells, and the slight increase in PS composition also contribute to the selective lytic activity of the diastereomers.

It is quite surprising that the diastereomers are not hemolytic at all despite the findings that they bind strongly and permeate zwitterionic membranes, like all L-amino acid lytic peptides which are highly hemolytic (*21*). A plausible explanation is that they bind first to the negatively charged glycocalix layer of erythrocytes and cannot diffuse and segregate easily within the zwitterionic membrane, because of the lack of a stable amphipathic structure, which contributes significantly to the partitioning into zwitterionic membranes (*32*). In contrast to the diastereomers, all L-amino acids or all D-amino acids with similar sequences can readily form stable amphipathic helices, and therefore can partition easily from the glycocalix layer into the zwitterionic cell membrane. Therefore, slight changes in the outer surface composition will not have a strong effect on their partitioning into the zwitterionic cell membrane. This is further demonstrated in the non-cell selective activity of LL-37 (Table 2) that perturbs the membranes in a manner similar to that of the diastereomers (Figure 2) but forms a stable helical structure (*22*). Note also that tumorigenic cells contain relatively large amounts of microvilli compared to normal cells that may serve as a trigger for macrophage recognition and promote phagocytosis of the cells (*7*). The microvilli will increase the surface area of the cells' membrane, and hence increase the amount of peptides on these cells (*34*).

The data also reveal that antimicrobial activity does not necessarily correlate with anticancer activity, since 12-mer diastereomeric antimicrobial peptides are devoid of anticancer activity up to 100 μM (data not shown) (*8*). In addition, the diastereomer of melittin has a potent antimicrobial activity, but is devoid of anticancer activity (*21*). Furthermore, it has been shown that the addition of positive charges to the N-terminus of antimicrobial peptides increases antimicrobial activity (*5*, *23*). Here, similar modifications were introduced by adding one or two lysines to the parental peptide, but apart from one type of cells, the anticancer activity did not change significantly. Interestingly, inversion of the sequence ($l^{3,6,13}k^{8,9}K_6L_9$), which should affect only the dipole moment, and hence the stability of the helical structure (based on FTIR spectroscopy), resulted in a significant decrease in activity (~4−8-fold) mainly toward the normal OL foreskin and NIH-3T3 cells.

The findings that the peptides bind similarly to mono- and bilayers of zwitterionic membrane and only slightly better (~2-fold) to negatively charged bilayers than to monolayers suggest that the inner leaflet does not contribute significantly to their binding. Therefore, the peptides do not interact with

the hydrophobic core of the membrane, and instead lie on the surface of the membrane. Peptides that insert into the inner leaflet of the membrane have been shown to bind bilayers much stronger than monolayers (~25-fold), as has been shown with the "pore forming" melittin (*35*). In this study, the ~2-fold increase in the level of binding of the diastereomers to negatively charged bilayers compared with monolayers could indicate that they translocate only slightly into the inner membrane via interaction with the lipid headgroups, as proposed by the carpet mechanism (*5*) and by others (*36*). The inability of the diastereomers to insert deeply into the hydrophobic core of the membrane is also supported by the FTIR studies (data not shown), which shows that the diastereomers did not affect significantly the lipid order of the membranes.

In summary, the diastereomeric peptides have a unique property by being highly active on the membranes of both normal and cancer cells which are predominantly zwitterionic, but yet they can discriminate between these cells. This is in contrast to most native antimicrobial peptides, which are highly active predominantly toward negatively charged membranes and therefore are less potent toward cancer cells. Cell selectivity is determined predominantly by an increase in the level of acidic components on the cancer cell wall but not by the slight increase in the level of PS in the outer surface of the cancer cell membranes. The data also indicate that there is a need for an amphipathic structure, an ideal helix or a distorted one, to confer high anticancer activity. Note that the addition of lysines to the N-terminus of the peptides to increase their net positive charge decreases the helical structure content, due to the effect on the dipole moment. However, the slight increase in their level of binding to the PS-containing membranes probably compensates for the reduction in the helical structure and therefore makes them as potent as the wild-type peptide $l^{3,10,13}k^{7,8}K_6L_9$.

From a therapeutically point of view, diastereomeric peptides should have several advantages over all L-amino acid or all D-amino acid lytic peptides. (1) They lack the diverse pathological and pharmacological effects induced by their parental all L-amino acid lytic peptides (*37*). (2) They preserve activity in serum and in the presence of proteolytic enzymes, whereas native peptides lose most or all of their activity (*8*). (3) The antigenicity of short fragments containing D,L-amino acids is dramatically reduced compared to those of their all L- or all-D-amino acid parent molecules (*38*). (4) In contrast to commercially available chemotherapeutic drugs, which act on specific targets, there is ample evidence that due to the drastic lytic effect caused by these peptides, it is difficult for the target cell to develop resistance. Therefore, these peptides may provide alternative solutions to multidrug resistance (MDR), a major cause of treatment failure in malignant disorders. Indeed, previous studies revealed that MDR cells are as sensitive as non-MDR cells to native antimicrobial peptides (*39*). Furthermore, the membrane disrupting activity of the peptides may be utilized to overcome MDR activity by increasing the permeability of cancer cells to conventional drugs. Overall, their simple composition and high anticancer activity provide a model for studying elements that determine selective lysis of cancer cells to develop new drugs for chemotherapeutic use.

REFERENCES

1. Smith, L. L., Brown, K., Carthew, P., Lim, C. K., Martin, E. A., Styles, J., and White, I. N. (2000) *Crit. Rev. Toxicol. 30*, 571−594.
2. Boman, H. G. (1995) *Annu. Rev. Immunol. 13*, 61−92.
3. Zasloff, M. (2002) *Nature 415*, 389−395.
4. Hancock, R. E., and Diamond, G. (2000) *Trends Microbiol. 8*, 402−410.
5. Shai, Y. (1999) *Biochim. Biophys. Acta 1462*, 55−70.
6. Matsuzaki, K. (1999) *Biochim. Biophys. Acta 1462*, 1−10.
7. Zwaal, R. F., and Schroit, A. J. (1997) *Blood 89*, 1121−1132.
8. Oren, Z., Hong, J., and Shai, Y. (1997) *J. Biol. Chem. 272*, 14643−14649.
9. Merrifield, R. B., Vizioli, L. D., and Boman, H. G. (1982) *Biochemistry 21*, 5020−5031.
10. Pouny, Y., and Shai, Y. (1992) *Biochemistry 31*, 9482−9490.
11. Allen, T. M., and Cleland, L. G. (1980) *Biochim. Biophys. Acta 597*, 418−426.
12. Oren, Z., and Shai, Y. (2000) *Biochemistry 39*, 6103−6114.
13. Surewicz, W. K., Mantsch, H. H., and Chapman, D. (1993) *Biochemistry 32*, 389−394.
14. Harrick, N. J. (1967) *Internal Reflection Spectroscopy*, Interscience, New York.
15. Ishiguro, R., Kimura, N., and Takahashi, S. (1993) *Biochemistry 32*, 9792−9797.
16. Mozsolits, H., Wirth, H. J., Werkmeister, J., and Aguilar, M. I. (2001) *Biochim. Biophys. Acta 1512*, 64−76.
17. Mozsolits, H., and Aguilar, M. I. (2002) *Biopolymers 66*, 3−18.
18. Schiffer, M., and Edmundson, A. B. (1967) *Biophys. J. 7*, 121−135.
19. Frohm, M., Agerberth, B., Ahangari, G., Stahle-Backdahl, M., Liden, S., Wigzell, H., and Gudmundsson, G. H. (1997) *J. Biol. Chem. 272*, 15258−15263.
20. Johansson, J., Gudmundsson, G. H., Rottenberg, M. E., Berndt, K. D., and Agerberth, B. (1998) *J. Biol. Chem. 273*, 3718−3724.
21. Oren, Z., and Shai, Y. (1997) *Biochemistry 36*, 1826−1835.
22. Oren, Z., Lerman, J. C., Gudmundsson, G. H., Agerberth, B., and Shai, Y. (1999) *Biochem. J. 341*, 501−513.
23. Bessalle, R., Haas, H., Goria, A., Shalit, I., and Fridkin, M. (1992) *Antimicrob. Agents Chemother. 36*, 313−317.
24. Verkleij, A. J., Zwaal, R. F., Roelofsen, B., Comfurius, P., Kastelijn, D., and Deenen, L. L. v. (1973) *Biochim. Biophys. Acta 323*, 178−193.
25. Frey, S., and Tamm, L. K. (1991) *Biophys. J. 60*, 922−930.
26. Jackson, M., and Mantsch, H. H. (1995) *Crit. Rev. Biochem. Mol. Biol. 30*, 95−120.
27. Cameron, D. G., Casal, H. L., Gudgin, E. F., and Mantsch, H. H. (1980) *Biochim. Biophys. Acta 596*, 463−467.
28. Oren, Z., and Shai, Y. (1998) *Biopolymers 47*, 451−463.
29. Papo, N., and Shai, Y. (2003) *Biochemistry 42*, 458−466.
30. Tossi, A., Sandri, L., and Giangaspero, A. (2000) *Biopolymers 55*, 4−30.
31. Cappelli, G., Paladini, S., and D'Agata, A. (1999) *Tumori 85*, S19−S21.
32. Ladokhin, A. S., and White, S. H. (1999) *J. Mol. Biol. 285*, 1363−1369.
33. Ohsaki, Y., Gazdar, A. F., Chen, H. C., and Johnson, B. E. (1992) *Cancer Res. 52*, 3534−3538.
34. Chan, S. C., Hui, L., and Chen, H. M. (1998) *Anticancer Res. 18*, 4467−4474.
35. Papo, N., and Shai, Y. (2003) *Biochemistry 42*, 458−466.
36. Matsuzaki, K., Murase, O., and Miyajima, K. (1995) *Biochemistry 34*, 12553−12559.
37. Abu-Raya, S., Bloch-Shilderman, E., Shohami, E., Trembovler, V., Shai, Y., Weidenfeld, J., Yedgar, S., Gutman, Y., and Lazarovici, P. (1998) *J. Pharmacol. Exp. Ther. 287*, 889−896.
38. Benkirane, N., Friede, M., Guichard, G., Briand, J. P., Van, R. M., and Muller, S. (1993) *J. Biol. Chem. 268*, 26279−26285.
39. Van der Schaft, P. H., Roelofsen, B., Op den Kamp, J. A., and Van Deenen, L. L. (1987) *Biochim. Biophys. Acta 900*, 103−115.

BI027212O